First principles calculation of the potential energy surface for the lowest-quartet state of H_3 and modelling by the double many-body expansion method

P. E. Abreu and A. J. C. Varandas*

Departamento de Química, Universidade de Coimbra, P-3049 Coimbra Codex, Portugal

We report a study of the potential energy surface for the lowest quartet state of H_3. At the *ab initio* level, restricted Hartree–Fock and full configuration interaction (FCI) calculations were performed with two extended Gaussian basis sets providing a detailed coverage of the molecule configuration space. A total of 102 geometries, both linear and nonlinear, have been examined. These calculated energies have then been partitioned into two-body and three-body Hartree–Fock energy components, and combined with two-body and three-body semiempirical models of the dynamical correlation energy to obtain a realistic double many-body expansion (DMBE) representation of the title potential energy surface. In conjunction with a previously reported DMBE potential energy surface for the two lowest-doublet states of H_3, this completes the set of potentials on which accurate dynamics calculations may be carried out for any collision process involving three ground-state hydrogen atoms. A number of FCI calculations have also been carried out to test the reliability of the modelled DMBE potential energy surface.

1 Introduction

H_3 is the simplest neutral polyatomic molecule, and hence it has long been a fertile testing ground for theoretical and experimental work. Although the potential energy surface for ground-doublet H_3 is known with chemical accuracy (<1 kcal mol^{-1}) from correlated *ab initio* electronic structure calculations,[1,2] (for further *ab initio* calculations, see refs. 3–5 and references therein), which have subsequently been used to calibrate a DMBE potential energy surface for this system,[2] no similar study has been reported for its lowest quartet state. However, knowledge of the potential energy surface for the title system may be of interest on several important practical grounds: (a) as a prototype for the formally similar repulsive interactions involving closed shell atoms or identical spin alkali metal trimers; (b) to define the three-body energy terms which arise on the many-body expansion[5] and DMBE[7,8] developments of the total potential, since $H_3(^4A')$ may, by the Wigner–Witmer rules, occur as a fragment on the dissociation of hydrogen-containing species, *e.g.*, $NH_3(^1A')$;[9] (c) to study atomic recombination and thermophysical properties of atomic hydrogen; (d) to complete, in conjunction with the DMBE potential energy surface reported[2] for the two lowest doublet states of H_3, the set of potentials on which the collision of three ground state hydrogen atoms may evolve and hence open the possibility for accurate dynamics calculations.

In this work we report a detailed *ab initio* study of the title system at the single-configuration self-consistent-field (SCF) and FCI levels. Thus, it may be viewed as an extension of unpublished results[10] in our group. To represent the one-particle basis functions we have chosen the extended-Gaussian basis set developed by Siegbahn and Liu,[1] which has been also adopted on the calculations for ground-doublet H_3 by Varandas *et al.*[2] We also choose the augmented correlation consistent basis of Dunning[11] (aug-cc-pVQZ) to provide a comparison. Energies are reported for 102 geometries cover-

ing various perimeters and shapes of the triangle formed by the three H atoms, being compared with previous *ab initio* molecular orbital calculations by Murrell, Varandas and Guest,[12] and first-order exchange perturbation calculations by Kolos and Lés.[13] With this information, a model representation has been built in which the SCF energies are functionally represented after being partitioned into two-body and three-body components. To these, the standard second order plus the non-additive third-order (Axilrod–Teller–Muto) dispersion energy components have been added semiempirically, such energy contributions being damped for charge-overlap effects at short and intermediate distances. Thus, our procedure follows the spirit of the DMBE[7,8,14–16] method.

The paper is organized as follows. In Section 2, we discuss the choice of coordinates. We present the results of the *ab initio* calculations in Section 3. Section 4 provides a description of the DMBE model including a description of the two-body terms. In Section 5 we present the potential energy surface and its features. A short summary of the work is in Section 6.

2 Coordinate system

For a system with high permutational symmetry such as $H_3(^4A')$, the potential energy surface must be symmetrical under exchange of the interatomic coordinates. This is most conveniently performed using symmetry coordinates adequate for the S_3 permutation group (for a survey, see ref. 6). Indeed, we may define the integrity basis polynomials

$$\Gamma_1 = Q_1$$

$$\Gamma_2 = Q_2^2 + Q_3^2$$
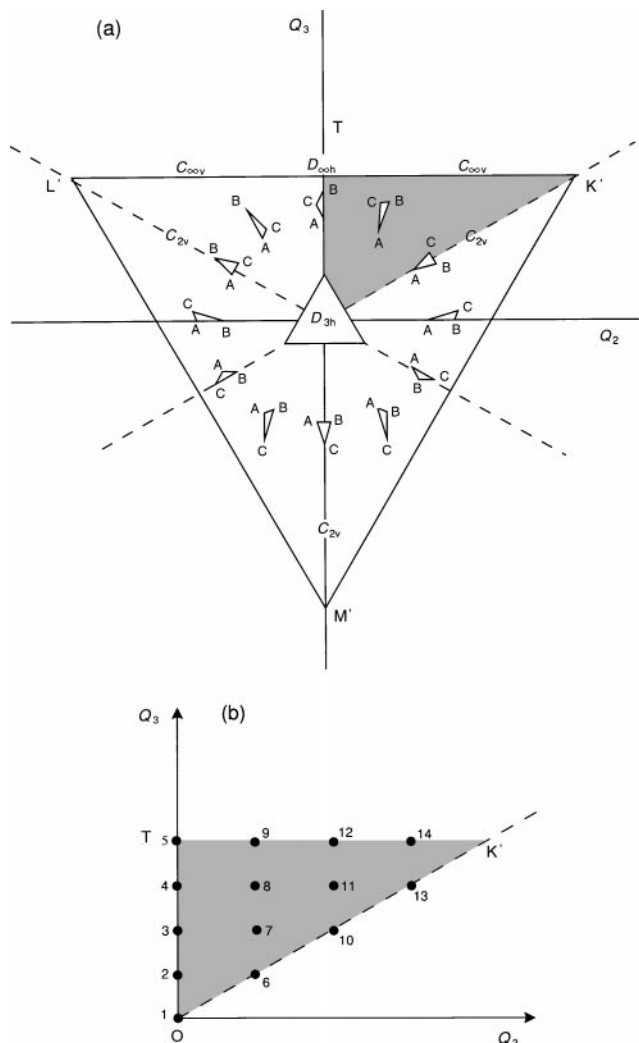
$$\Gamma_3 = Q_3(Q_3^2 - 3Q_2^2) \tag{1}$$

Fig. 1 (a) Representation of the geometries considered on the present calculation, for a fixed perimeter P or Q_1, $Q_1 = \sqrt{1/3}P$. (b) Relation between the symmetry coordinates Q_i and the shape space accessible to the molecule.

where Q_i ($i = 1$–3) are symmetry coordinates defined by

$$Q_1 = \frac{1}{\sqrt{3}} (R_1 + R_2 + R_3)$$

$$Q_2 = \frac{1}{\sqrt{2}} (R_2 - R_3)$$

$$Q_3 = \frac{1}{\sqrt{6}} (2R_1 - R_2 - R_3) \tag{2}$$

The reader may easily verify that the basis polynomials of eqn. (1) are totally symmetric under permutation of the coordinates, while being referred to ref. 17 and references therein for further details. For a constant perimeter, the symmetry of the problem therefore implies that a path encircling the origin ($Q_2 = Q_3 = 0$) spans all possible distortions of the triangle formed by the three atoms. The symmetries covered in such distortions are illustrated by the inner ABC triangles displayed in Fig. 1(a). Also indicated in the outer K'L'M' triangle are the loci of the most relevant symmetrical arrangements of the three atoms. Thus, for a fixed molecular perimeter, the symmetry of the problem implies that one is just required to perform calculations covering one sixth of the physical space to generate the full potential energy surface; see Fig. 1(b). The remaining geometries for the same perimeter are symmetry related to the calculated ones, and hence need not specific consideration if the model potential function to be calibrated from such data has built-in the proper symmetry of the full potential. Note that, because the potential energy surface for the lowest quartet state of H_3 is analytic everywhere, the potential function need not consider any of the non-analytic terms discussed elsewhere,[17,18] namely terms involving $|\Gamma_2|^{1/2}$ and $|\Gamma_3|^{3/2}$.

3 *Ab initio* calculations

Previous MO calculations on the title system have, to our knowledge, been reported only by Murrell, Varandas and Guest[12] (MVG) who carried out SCF and SCF CI calculations using a double zeta Slater-type orbital basis set. Energies were reported by those authors for 27 geometries covering only C_{2v}, or higher symmetries. Most recently, Korona *et al.*[19] reported a FCI study of the title system employing an extended basis set. In the present work we provide a detailed coverage of the $H_3(^4A')$ potential energy surface, which encompasses a wide range of geometries. The extended Gaussian basis set due to Siegbahn and Liu,[1] which has been optimized for the ground-doublet surface of H_3, has been utilized. In addition, the augmented correlation consistent basis of Dunning[11] (aug-cc-pVQZ) was used in order to provide a comparison. All *ab initio* calculations were performed using the GAMESS[20] code. Unless mentioned otherwise, atomic units were used in this work: 1 a_0 (bohr) $= 0.529\,177 \times 10^{-10}$ m; 1 E_h (hartree) $= 2625.47$ kJ mol^{-1}.

3.1 SCF calculations

Support for the use of the Siegbahn–Liu basis set comes from a comparison of the present results for $H_2(b\,^3\Sigma_u^+)$ with those obtained using the more extended Gaussian basis sets published by Lewchenko *et al.*,[21] and Dunning.[11] Table 1 reports this comparison. Also given for comparison are the MVG results at the SCF level. Two remarks can be made from Table 1. The first one concerns the good agreement of all four sets of calculations among each other. Thus, we believe that the present calculations can be as reliable as those of

Table 1 Restricted Hartree–Fock interaction energies, in μE_h, for $H_2(b\,^3\Sigma_u^+)$

R	MVG[12]	This work[a]	This work[b]	This work[c]	Eqn. (8)
2.0	107430.13	107184.94	107105.63	107120.82	110287.23
4.0	7545.14	7529.93	7522.77	7534.33	8311.08
6.0	359.38	358.69	357.91	358.83	393.81
7.0	70.24	70.16	69.88	70.13	77.55
8.0	13.03	12.99	12.84	12.99	14.80
10.0	0.38	0.38	0.31	0.40	0.48

[a] Using the Gaussian basis set of Siegbahn and Liu.[1] [b] Using the Gaussian basis set of Dunning.[11] [c] Using the Gaussian basis set of Lewchenko *et al.*[21]

Table 2 A summary of the geometries used for the *ab initio* calculations, and relevant included angles in degrees (for C_{2v} geometries only)

Shape index	Included angle	Symmetry
1	60	D_{3h}
2	73.74	C_{2v}
3	91.17	C_{2v}
4	115.50	C_{2v}
5	180	$D_{\infty h}$
6	38.94	C_{2v}
7	nr[a]	C_s
8	nr[a]	C_s
9	180	$C_{\infty h}$
10	23.07	C_{2v}
11	nr[a]	C_s
12	180	$C_{\infty h}$
13	10.43	C_{2v}
14	180	$C_{\infty h}$

[a] nr = not relevant.

MVG (based on a STO basis set) even at reasonably large interatomic separations. The other observation refers to the quality of the four Gaussian basis sets, which give very similar results. We conclude that the Siegbahn–Liu basis set is quite adequate for the purpose of the present work albeit being significantly smaller than that of Lewchenko *et al.*[21] Thus, it will be employed for the remaining calculations reported in this work.

3.2 FCI calculations

For the purpose of comparison we have also carried out some FCI calculations on selected geometries (included angles of 60° and 180°) using the aug-cc-pVQZ basis set.

3.3 Results

All SCF calculations for the lowest quartet state of H_3 are summarized in a table deposited as electronic supplementary information.† In this table, every geometry carries a sequencial number defined as follows. For each of the fourteen shape-types indicated in Fig. 1(b), the numbering is made according to increasing perimeter, P. Thus, the point number,

† Available as electronic supplementary information. See http://www.rsc.org/suppdata/cp/b0/b000464m

N_p, obeys the formula $N_p = 7N_s + (P/3 - 8)$, where N_s denotes the shape-index assigned in Fig. 1. For example, the D_{3h} geometry corresponding to the lowest perimeter ($P = 6$ a_0) is given the number 1 while that for the next shape-index with the same perimeter is given the number 8, and so Table 2 summarizes the correspondence between these shape-indexes and the symmetry attributes of the corresponding molecular structures. Because the counterpoise corrections for BSSE were very small for H_2, and also because there is no unique way of correcting for them in a polyatomic calculation,[22] they have also not been considered for $H_3(^4A')$. Finally, Table 3 compares, for geometries of C_{2v}, or higher symmetry, the results of the present work with those from previous first principles calculations available in the literature.[12,13] As seen from columns two and three of Table 3, the agreement with the MVG results is quite satisfactory.

4 DMBE representation of the potential energy surface

The dissociation scheme for the lowest quartet state of $H_3(^4A')$ is

$$H_3(^4A') \rightarrow \begin{cases} H(^2S) + H_2(b\,^3\Sigma_u^+) \\ 3H(^2S) \end{cases} \qquad (3)$$
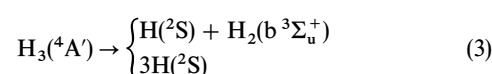
which suggests that the potential energy surface can be represented by a single-valued function over the complete molecular configuration space.

Within the framework of the DMBE method, the potential energy function is written in the form

$$V = V_{EHF}(\boldsymbol{R}) + V_{dc}(\boldsymbol{R}) \qquad (4)$$

where V_{EHF} is the geometry-dependent extended Hartree–Fock energy contribution, V_{dc}, represents the dynamical correlation, and $\boldsymbol{R} = (R_1, R_2, R_3)$ is a collective variable. The EHF energy is then modelled from available *ab initio* calculations (in our case restricted Hartree–Fock energies, simply abbreviated as HF) using a flexible enough functional form. Note that in the specific case of the present work the HF energy includes exactly all nondynamical correlation effects, and hence we indistinguishably refer to this energy as HF or EHF in the foregoing discussion. In turn, the dc energy is modelled semi-empirically from the long-range dispersion energy coefficients which, for the title system, are accurately known from theoretical calculations. Because these coefficients are calculated from the isolated fragments alone, they need to be modulated

Table 3 Analysis of the restricted Hartree–Fock interaction energy, in μE_h, for some D_{3h} (first five entries) and $D_{\infty h}$ (last seven entries) geometries, and comparison of the calculated ratios of the present work with the results from previous studies

	V_{HF}		$V_{HF}^{(2)}$	$V_{HF}^{(3)}$	$\eta_{HF} \times 10^2$		
R	This work	Ref. 12	This work	This work	This work	Ref. 12	Ref. 13
D_{3h}							
2	255875.31	256524.37	321549.41	−66129.08	−20.56	−20.41	−24.63
3	71579.59	—	89890.66	−18996.32	−21.13	—	−20.53
4	19137.57	19192.54	22589.38	−3544.77	−15.69	−15.21	−14.53
5	4637.69	—	5142.15	−516.86	−10.05	—	−8.99
6	1015.80	1017.67	1076.07	−62.61	−5.81	−5.62	−5.03
$D_{\infty h}$							
1.5	373762.94	—	422648.46	−46029.77	−9.90	—	—
2.25	171504.48	—	161094.79	9463.47	5.87	—	—
3	63858.62	—	60285.79	4014.86	6.66	—	4.47
3.75	22204.66	—	21508.38	617.33	2.87	—	—
4.5	7378.82	—	7270.88	81.87	1.13	—	—
5.25	2349.90	—	2335.55	10.26	0.44	—	—
6	719.06	720.22	717.32	1.23	0.17	0.20	0.14

at short distance through the use of universal charge-overlap damping functions, which vary smoothly from 0 (or a value close to zero) at $R = 0$ to 1 at $R = \infty$.

Following the usual procedure, the terms in eqn. (4) are written in the form of the many-body expansion[6]

$$V_{EHF} = \sum_{i=1}^{3} V_{EHF,i}^{(2)}(R_i) + V_{EHF}^{(3)}(\boldsymbol{R}) \tag{5}$$

$$V_{dc} = \sum_{i=1}^{3} V_{dc,i}^{(2)}(R_i) + V_{dc}^{(3)}(\boldsymbol{R}) \tag{6}$$

where the superscripts denote the various two-body and three-body energy terms. Because we have a single-valued surface, the zero of energy in eqns. (5) and (6) is taken as the energy of the three isolated H atoms. The following sections give the details of the functional forms used to represent the various terms in eqns. (5) and (6).

4.1 Two-body energy terms

As usual, the potential curve for each two-body fragment is based on the EHFACE2U[23,24] (extended Hartree–Fock approximate correlation energy) model, which shows the correct behaviour at $R \to 0$ and $R \to \infty$. First, we consider the curve for the ground singlet of H_2. This assumes the form

$$V^{(2)} = V_{EHF}^{(2)}(R) + V_{dc}^{(2)}(R) \tag{7}$$

where

$$V_{EHV}^{(2)} = -DR^{-1}\left(1 + \sum_{i=1}^{3} a_i s^i\right)$$
$$\times \exp[-\gamma(s)s] + \chi_{exc}(R)V_{exc}^{asym}(R) \tag{8}$$

and

$$\gamma = \gamma_0[1 + \gamma_1 \tanh(\gamma_2 s)] \tag{9}$$

Thus, $V_{exc}^{asym}(R)$ is the leading contribution[25–27] of the exchange energy at asymptotic distances, the damping function of which is represented by χ_{exc}. In addition, $s = R - R_e$ is the displacement coordinate from the equilibrium geometry, R_e, and D, γ_i ($i = 0$–2) and a_i ($i = 1$–3) are parameters which can be determined[23] from a fit to *ab initio* or experimental data. For the asymptotic exchange energy of H_2 the theoretical data reported in the literature was used.[24,27] This assumes the form

$$V_{exc}^{asym} = \tilde{A}R^{\tilde{a}}\left(1 + \sum_{i=1} \tilde{a}_i R_i\right)\exp(-\tilde{\gamma}R) \tag{10}$$

where $\tilde{A}$, $\tilde{a}$, $\tilde{a}_i$ and $\tilde{\gamma}$ are theoretical parameters related to the asymptotic behaviour of the wave function through some molecular integrals.[27] The damping function $\chi_{exc}(R)$ in this case has been approximated by $\chi_6(R)$. The value of the parameters in eqns. (8)–(10) are collected in Table I of ref. 28.

In turn, the dynamical correlation energy in eqn. (8) is written as

$$V_{dc}^{(2)} = -\sum_n C_n \chi_n(R) R^{-n} \tag{11}$$

where the damping functions are given by[29]

$$\chi_n = [1 - \exp(-A_n R/\rho - B_n R^2/\rho^2)]^n \tag{12}$$

and $A_n = \alpha_0 n^{-\alpha_1}$ and $B_n = \beta_0 \exp(-\beta_1 n)$ are auxiliary functions;[29] $\alpha_0 = 16.36606$, $\alpha_1 = 0.70172$, $\beta_0 = 17.19338$, $\beta_1 = 0.09574$. Moreover, ρ is a scaling parameter defined by $\rho = (5.5 + 1.25R_0)$, $R_0 = 2(\langle r_X^2 \rangle^{1/2} + \langle r_Y^2 \rangle^{1/2})$ is the LeRoy[30] parameter, and $\langle r_X^2 \rangle$ is the expectation value of the squared radii for the outermost electrons in atom X (similarly for the

other interacting atom Y). All relevant parameters are numerically defined in Table II of ref. 28. Using the above description of the ground singet curve the $H_2(a\,^3\Sigma_u^+)$ potential is then obtained as[28]

$$^3\Sigma_u^+ = {}^1\Sigma_g^+ + \Delta V(R) + \Delta V_{exc}^{asym}(R) \tag{13}$$

where $\Delta V_{exc}^{asym}(R)$ represents the energy difference between the ground state singlet and lowest triplet curves at asymptotic distances, and $\Delta V(R)$ is an additional term which accounts effectively for the remaining part of the short range energy. This has been written as[28]

$$\Delta V(R) = \exp\left(-\sum_{i=0}^{m} b_i R^i\right) \tag{14}$$

with the least squares parameters b_i ($i = 0$–m) being determined from a fit to the exact Kolos–Wolniewicz[31] *ab initio* energies for nonzero R values, and the atomic helium energy splitting $E(He,\,^3P) - E(He,\,^1S) = 169086.87$ cm^{-1} for $R = 0$. Furthermore, m has been chosen subject to the requirement $m \geqslant 2$ which warrants the proper behaviour of the exchange energy at asymptotic separations. The optimum values of the least-square parameters in eqn. (14) are given in Table III of ref. 28. The agreement with the exact Kolos–Wolniewicz[31] energies is good.[28] Since the agreement with the *ab initio* energies from this work is also good, we deemed unnecessary any refinement of the extended Hartree–Fock two-body energy curve reported in ref. 28.

4.2 Three-body EHF energy term

The three-body extended Hartree–Fock energies were determined by subtracting the two-body EHF energies [given by eqn. (8)] for the specific distances involved in the triatomic from the computed HF triatomic interaction energies (see the electronic supplementary information†). These three-body EHF energies were then fitted to the form

$$V_{EHF}^{(3)} = P(\Gamma_1, \Gamma_2, \Gamma_3) \times T(\Gamma_1) \tag{15}$$

where P is a complete fourth-order polynomial defined by

$$P = \sum_{\substack{i,j,k=0 \\ i+2j+3k \leqslant 4}} c_{ijk} \Gamma_1^i \Gamma_2^j \Gamma_3^k \tag{16}$$

and T is a range determining factor given by

$$T = 1 - \tanh(\gamma_0 + \gamma_1 \Gamma_1) \tag{17}$$

The determination of the involved fitting parameters was then carried out by the least-squares method using the LMDER subroutine of the MINPACK[32,33] package. The following procedure has been adopted. Of the 102 points (gathered in the electronic supplementary information†), 32 carried a weight given by eqn. (18) during the least-squares fitting procedure while the remaining points were given a weight of zero. Thus, these latter points served only to test the reliability of the resulting least-squares functional form at the corresponding geometries. The emphasis has therefore been on reliability while keeping simplicity of the functional form at the highest possible level compatible with the accuracy requirements. Thus, better fits could probably be achieved by using higher-order polynomial forms, although this approach was not pursued here. Note that, in the Gaussian-type distributions used for the least-squares weighting,

$$\omega_i = 10^{-3} \frac{\exp[-2(E_i - E_{ref})^2]}{E_i - E_a} \tag{18}$$

E_i stands for the total electronic energy of the *i*-th point, $E_a = -1.49999729\,E_h$ is the energy for three isolated hydrogen atoms, and $E_{ref} = 1.4\,E_h$ is an arbitrarily defined reference
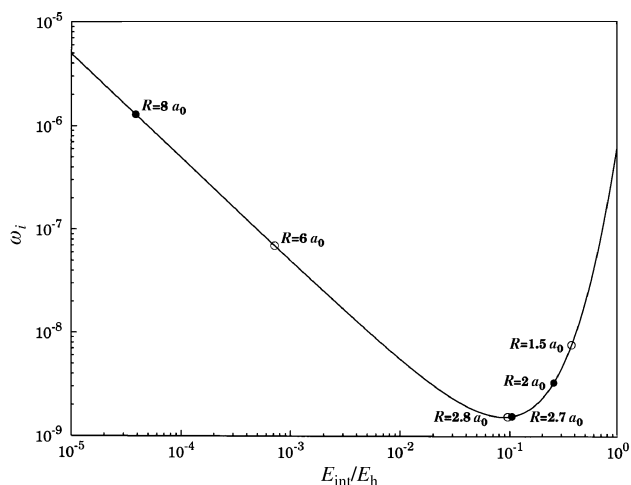
Fig. 2 Plot of the weighting function in eqn. (14) as a function of the interaction energy. The open circles refer to $D_{\infty h}$ and the full circles to D_{3h} geometries.

energy. Fig. 2 shows this weighting function as a function of the interaction energy. It is seen that we tried to avoid weighting excessively both highly repulsive geometries and geometries falling in the very weak interaction region after the van der Waals minimum. Note that for these geometries the calculated three-body energies are expected to be relatively less accurate. In fact, for large separations between the subsystems, the Hartree–Fock densities may loose reliability[1] due to being based on Gaussian orbitals, which die-off too rapidly. Yet, we emphasize that our results on the diatomic fragments (Table 1) agree, at the largest distance considered of $R = 10\ a_0$, within $\sim 5\%$ with the SCF calculations of MVG, which used a basis set of Slater-type orbitals. On the other hand, at the high repulsive regions (for which any $R_i < 0.5\ a_0$), the EHF term of our diatomic potential function becomes less reliable, as it does not show the proper coulombic behaviour at the collapsed diatomic limit close to the united-atom.[23] As a result, any errors caused in these high-energy regions due to a poor description of the two-body EHF potential curves tend to be compensated through distortion of the EHF three-body energy form, which is modelled to the three-body energies resulting from subtraction of the two-body EHF energies from the computed triatomic SCF energies. The least-squares coefficients so-obtained are numerically defined in Table 4 while the relative errors are given in column 8 of the table provided as electronic supplementary information.† It is seen from this table that the current functional form accurately represents the 32 *ab initio* interaction energies (which correspond to the actually fitted three-body data points), giving a root-mean-square error of rms = $6.30 \times 10^{-4}\ E_h = 0.40$ kcal mol^{-1}. It provides also a good extrapolation for the non-fitted geometries. Indeed, if only very repulsive geometries with an energy higher than $0.5\ E_h$ are discarded, one gets rms = 1.33×10^{-3} $E_h = 0.84$ kcal mol^{-1}. Thus, our function has chemical accuracy over the complete configuration space of the triatomic system although containing only eleven linear and two nonlinear adjustable parameters.

An interesting source of information comes from the so-called non-additivity ratios,[12,13] which are generally defined as

$$\eta = \frac{V^{(3)}}{V^{(2)}} \tag{19}$$

Fig. 3 shows the HF ratios so-obtained for various symmetrical arrangements (in all cases there are at least two equal bond distances, *i.e.*, the symmetry is C_{2v} or higher, namely $D_{\infty h}$ or D_{3h}) of the three atoms. It is seen that the functional form of the present work provides a good representation of these ratios by smoothly connecting all the calculated points. Moreover, as shown in Table 3 and Fig. 4, there is good agreement between the non-additivity ratios of the present work and those of previous theoretical studies, which utilized both variational calculations[12] similar to those of the present work, and first-order exchange perturbation theory.[13]

4.3 Three-body dynamical correlation energy term

We represent this energy contribution by the non-expanded form of the triple-dipole dispersion energy, also referred to as the Axilrod–Teller–Muto term.[34-36] This is the leading energy term in the dispersion expansion arising in third-order of long-range perturbation theory

$$V^3_{\text{dis}} = \sum_{l_1 l_2 l_3 \geqslant 1} C_{l_1 l_2 l_3} W_{l_1 l_2 l_3}(\alpha_1 \alpha_2\ \alpha_3)$$
$$\times R_1^{-l_1-l_2-1} R_2^{-l_2-l_3-1} R_3^{-l_3-l_1-1} \tag{20}$$

where $C_{l_1 l_2 l_3}$ are the well known dispersion coefficients, which are independent of the geometrical arrangement of the three atoms, and $W_{l_1 l_2 l_3}$ are shape factors which depend on the included angles of the triangle formed by the three atoms. For example, the $W_{l_1 l_2 l_3}$ factors for the three leading terms arising
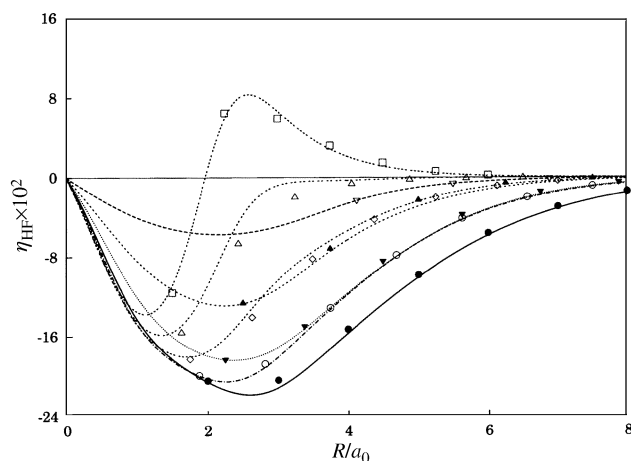

Fig. 3 HF non-additivity ratios for C_{2v} geometries, or higher symmetries as a function of R (characteristic distance), keeping fixed the included angle. Lines refer to the fitted potential. Key: ●, —— 60°; ▽, – – – 10°; ▲, - - - - 23°; ▼, · · · · 39°; ○, – · – · 74°; ◇, – · · – 91°; △, - - - - - - 116°; □, - - - - - - 180°.

Table 4 Numerical definition of the coefficients in eqns. (16) and (17)[a]

$c_{000}/E_h = -1.6994874(-1)$	$c_{100}/a_0^{-1} = 6.2332434(-2)$	$c_{200}/a_0^{-2} = -1.3869118(-3)$
$c_{010}/a_0^{-2} = 2.3304068(-3)$	$c_{300}/a_0^{-3} = 1.8998458(-3)$	$c_{110}/a_0^{-3} = 1.0563875(-4)$
$c_{001}/a_0^{-3} = -7.4016941(-3)$	$c_{400}/a_0^{-4} = 5.5008135(-4)$	$c_{101}/a_0^{-4} = 1.4392969(-4)$
$c_{210}/a_0^{-4} = 1.0975665(-4)$	$c_{020}/a_0^{-4} = 5.5536880(-6)$	
$\gamma_0 = -3.5994854(0)$	$\gamma_1 = 7.4851103(-1)$	

[a] Given in parentheses are the powers of 10 by which the numbers should be multiplied, *e.g.*, $c(d) = c \times 10^d$.
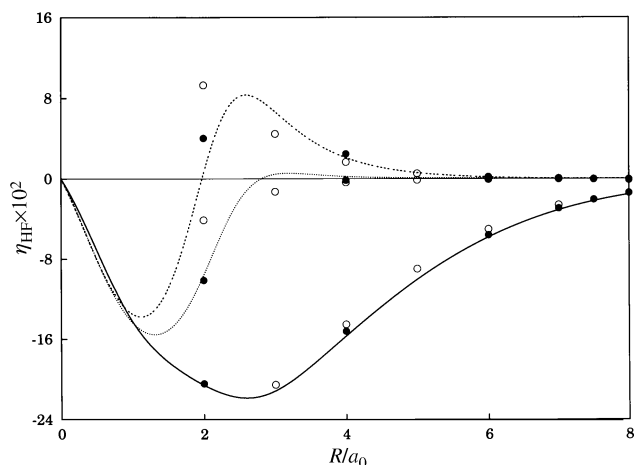
Fig. 4 Comparison of the HF non-additivity ratios for geometries with higher than C_{2v} symmetry as a function of R. The lines are the DMBE results. Also shown for comparison are the theoretical results of MVG (closed circles) and Kolos et al. (open circles). Key: —— 60°; ···· 120°; – – – 180°.

in this expansion assume the form[36]

$$W_{111} = 3(1 + 3 \cos \alpha_1 \cos \alpha_2 \cos \alpha_3) \qquad (21)$$

$$W_{112} = \tfrac{3}{16} \left[3(\cos \alpha_1 - 25 \cos 3\alpha_3) \right.$$
$$\left. + 6 \cos(\alpha_1 - \alpha_2)(3 + 5 \cos 2\alpha_3) \right] \qquad (22)$$

$$W_{122} = \tfrac{15}{64} \left[3(\cos \alpha_1 + 5 \cos 3\alpha_1) \right.$$
$$+ 20 \cos(\alpha_2 - \alpha_3)(1 - 3 \cos 2\alpha_1)$$
$$\left. + 70 \cos 2(\alpha_2 - \alpha_3)\cos \alpha_1 \right] \qquad (23)$$

with formulae for the cases $(l_1 l_2 l_3) = (211)$, (121), (212) and (221) being, of course, given by cyclic permutation of the suffixes (see ref. 36 for the general formula from which all these formulas can be derived). Unfortunately, except for the leading (111) term, no calculation of the non-expanded non-additive dispersion energy has been carried out, and hence only for the former have the effects of charge-overlap (not included in eqn. (20)) been calculated[37] and analytically modelled[38] through a suitable damping function. Note, however, that the contributions from the higher-order terms in the summation of eqn. (20) are expected to be significantly smaller than that of the leading term, which, as shown below, contributes itself only negligibly (say <1%) to the total interaction energy except at the long range regions of the potential after the van der Waals
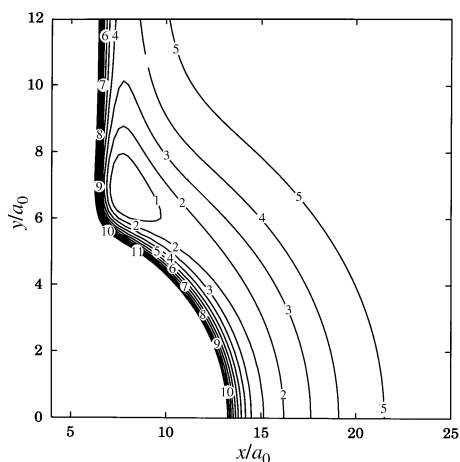
minimum. Thus, they were deemed irrelevant for the purposes of the present work, particularly because they would increase the complexity of the final potential without contributing significantly to improve its reliability. It should also be noted that there are additional non-additive contributions which arise in second and higher-orders of long range perturbation theory but which vanish exponentially at the asymptotic limit. O'Shea and Meath[37] found that such terms can compete with the non-expanded triple-dipole result for all but values of R somewhat larger than the van der Waals minimum in H_2 (b $^3\Sigma_u^+$), i.e., $R_m \simeq 7.82$ a_0. Particularly important in this competition with the terms that vary asymptotically as an inverse power of the interatomic separations are terms which are exponentially decreasing functions of only one interatomic distance. However, their contribution should be most important for small values of R where one also expects that the HF energy contribution probably dominates.

Meath and Azis[39] have given a detailed discussion on the possible non-additive contributions to the binding energy in van der Waals molecules such as the inert gas trimers. An interesting observation from their work is the fact that by taking as the only representatives of the non-additive interactions the undamped dispersion (111), (112), (122), (113) and (222) terms they obtained perfect agreement between the calculated and experimental values on the crystal binding energies of neon, argon, krypton and xenon. However, proper inclusion of the first-order three-body exchange effects considerably impaired agreement with experiment.[39] (Of course, the first-order energy arising in exchange perturbation theory differs from the HF energy only in that the latter contains a small non-additive induction-type energy.[40]) Meath and Azis[39] have been unable to identify the energy contribution which seems to cancel the effect of the exchange non-additive energies.

In summary adding together the three-body Hartree–Fock energy and the three-body dynamical correlation as approximated by the triple-dipole dispersion energy (suitably damped to account for charge overlap effect) gives probably the simplest reliable representation of the full three-body energy for the lowest quartet state of H_3. This has been the approach followed in the present work, having chosen the non-expanded triple-dipole form of Varandas[38] to represent the three-body dynamical correlation energy. This is written as[38]

$$V_{dc}^{(3)} = C_9[1 + 84.72 \exp(-10.84X) + 3 \cos \alpha_1 \cos \alpha_2 \cos \alpha_3]$$

$$\times \frac{[1 - \exp\{-3.20(1 - 0.16\Gamma_{123})X[1 + 1.51(1 + 0.69\Gamma_{123})X]\}]^9}{R_1^3 R_2^3 R_3^3}$$

$$(24)$$

where

$$\Gamma_{123} = \sum_{i=3}^{3} \sin \alpha_i \qquad (25)$$

$$X^3 = \prod_{i=1}^{3} x_i \qquad (26)$$

$$x_i = \frac{2R_i}{R_{m,i} + 2.5R_{0,i}} \quad (i = 1, 2, 3) \qquad (27)$$

and the long range dispersion coefficient $C_9 = 21.6425$ E_h a_0^9 assumes the appropriate value for three interacting H atoms.[37,41]

5 Features of the potential energy surface

The features of the complete $H_3(^4A')$ DMBE potential energy surface have been examined graphically by performing various
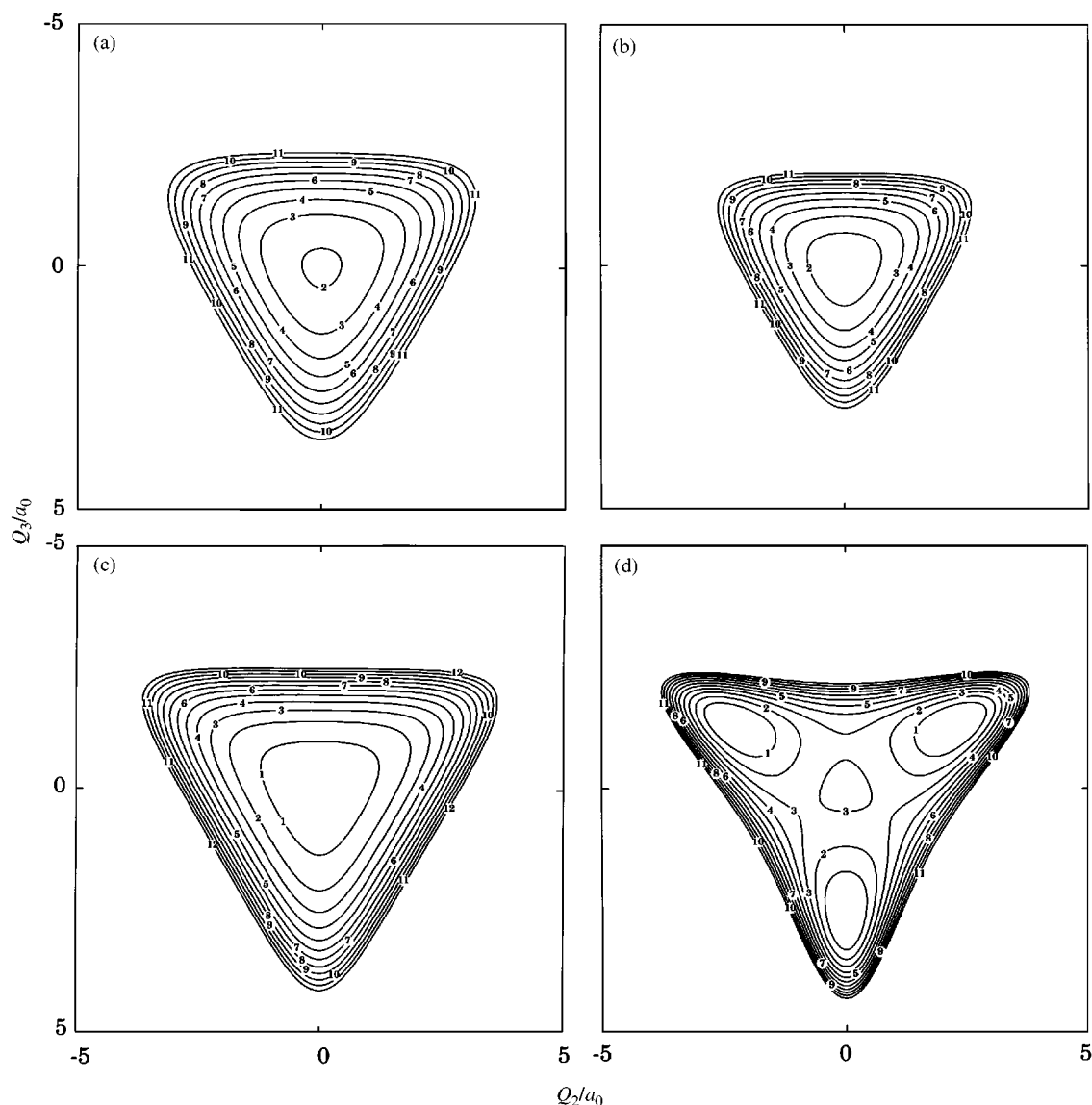

Fig. 5 Contour plot of the total interaction energy for the C_{2v} insertion of H(^{2}S) into H_2(b $^3\Sigma_u^+$). The contours are evenly spaced by 10^{-5} E_h, starting at -5×10^{-5} E_h.

Fig. 6 Triangular plots of the DMBE potential energy surface for the lowest quartet state of H_3 at fixed molecular perimeters: (a) 18, (b) 21, (c) 23.34 (this corresponds to the absolute minimum of the potential) and (d) 27 a_0. Contours start at -43.34 μE_h, with the spacing between consecutive contours being (a) 600, (b) 60, (c) 1, (d) 1.25 μE_h. Note that the lowest contour in (a) and (b) is contour 2. Except for plot (d) where the minimum occurs at C_{2v}, all others have a D_{3h} structure as the minimum.
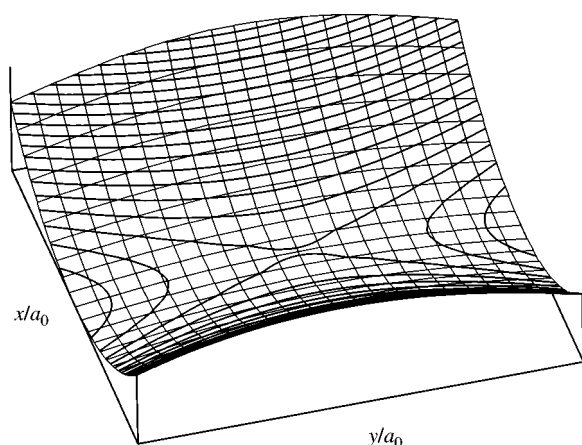

Fig. 7 Perspective view of the total interaction energy for a ground state hydrogen atom moving around a $H_2(b\,^3\Sigma_u^+)$ molecule, fixed at the geometry of lowest energy with the origin at the centre of the bond.

kinds of plots. These also allowed us to establish whether the potential had the desired features of smoothness, absence of unphysical holes, and so on.

Fig. 5 shows a contour plot of the total interaction energy for the C_{2v} insertion of $H(^2S)$ into $H_2(b\,^3\Sigma_u^+)$. It is seen that there is only one single minimum corresponding to a very weakly bound van der Waals structure with an included angle of $\alpha = 60°$. Indeed, a numerical search of the absolute minimum of the current potential energy surface has further indicated that it corresponds to a D_{3h} structure with a characteristic bond length of $R = 7.781$ a_0 and binding energy (relative to the three-atom asymptote) $E = -6.2475 \times 10^{-5}$ $E_h(164$ J mol$^{-1})$. Moreover, the calculated fundamental frequencies have been found to be ~ 43 cm^{-1} for the totally symmetric normal-mode vibration (breathing mode of a_1' symmetry), and ~ 31 cm^{-1} for the doubly degenerate (e′) vibrations. Of course, due to the large anharmonicity of the $H_3(^4A')$ potential energy surface in the vicinity of the minimum, this does not imply that the potential supports a
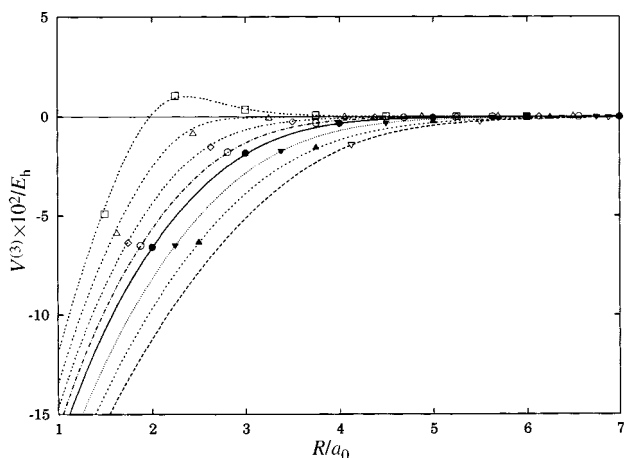
Fig. 8 Three-body extended Hartree–Fock energy for geometries of C_{2v} symmetry or higher, as a function of characteristic bond distance. The points are the *ab initio* energies of this work while the DMBE results are represented as lines. Key: ●, —— 60°; ▽, – – – 10°; ▲, - - - - 23°; ▼, ···· 39°; ○, –·–·– 74°; ◇, - - - - - - 91°; △, - - - - - - 116°; □, - - - - - - - - 180°.
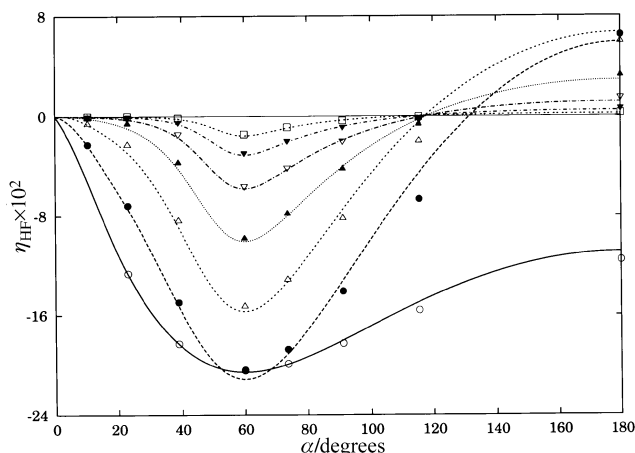

Fig. 9 Hartree–Fock non-additivity ratios for geometries of C_{2v} or higher symmetry having the same perimeter as a function of the included angle. The points correspond to the calculations and the lines to the DMBE potential. Key: ○, —— 6 a_0; ●, – – – 9 a_0; △, - - - - 12 a_0; ▲, ···· 15 a_0; ▽, –·–·– 18 a_0; ▼, –·–·– 21 a_0; □, - - - - - - 24 a_0.
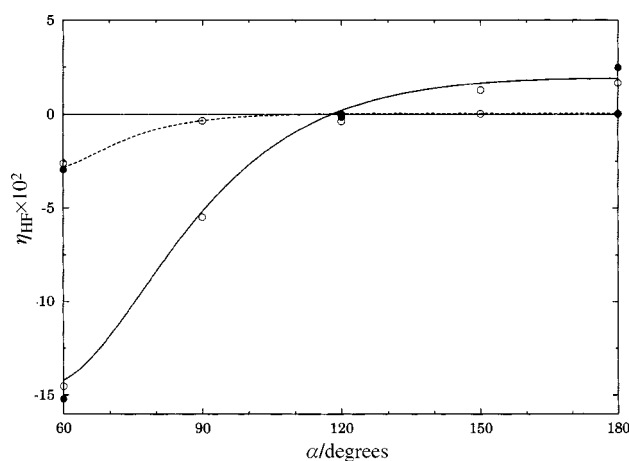

Fig. 10 Angular dependence of the HF non-additive ratios, as a function of the included angle for geometries of symmetry C_{2v} or lower symmetry, considering the value of R (characteristic distance) as constant. The lines are the DMBE results of this work: —— 4 a_0; – – – 7 a_0. Key for points: ●, MVG;[12] ○, Kolos and Lés.[13]

Table 5 Analysis of the FCI interaction energy and non-additivity ratios, in μE_h, for some D_{3h} (first four entries) and $D_{\infty h}$ (last five entries) geometries, and comparison of the calculated FCI ratios of the present work for the Siegbahn–Liu and Dunning basis sets

R	Siegbahn–Liu[1] $V^{(3)}$	η	aug-cc-pVQZ[11] $V^{(3)}$	η
D_{3h}				
3.0	−18432.59	−21.76	−18384.61	−21.88
4.0	−3454.21	−16.87	−3399.28	−17.07
5.0	−507.60	−11.76	−475.85	−12.01
6.0	−63.48	−8.23	−52.74	−9.16
$D_{\infty h}$				
3.0	3618.82	6.38	3677.54	6.54
3.8	702.88	3.56	718.81	3.73
4.5	—	—	111.13	1.83
5.3	—	—	13.91	0.82
6.0	1.22	0.24	1.13	0.30

bound state. Indeed, the analysis of the relative importance of the various contributions to the potential energy suggests that this minimum is essentially determined by the two-body potentials alone, which are themselves unbound.

The full symmetry of the $H_3(^4A')$ potential energy surface is displayed in Fig. 6, which shows a triangular plot for fixed molecular perimeters of 18, 21, 23.34 [this is the perimeter of the structure corresponding approximately to the absolute minimum of the $H_3(^4A')$ potential energy surface of the present work], and 27 a_0. The notable feature from these plots (see Fig. 7(c)] is clearly the existence of a single van der Waals minimum with threefold symmetry. Note also that the most stable structure for perimeters smaller than about 27 a_0 has D_{3h} geometry while for this and larger perimeters it has C_{2v} geometry with the D_{3h} point being a maximum. This is a clear manifestation that the three-body triple-dipole dispersion energy only dominates for such large perimeters (see also ref. 12).

A perspective view of the total interaction energy for a ground state hydrogen atom moving around a $H_2(b\,^3\Sigma_u^+)$ molecule, which is fixed at its geometry of lowest energy ($R_m = 7.82\ a_0$) with the centre of the bond at the origin, is displayed in Fig. 7. The very weak van der Waals minimum of the triatomic is apparent at the bottom of the highly repulsive hills while the energetically favourable path for attacking the diatomic is seen to be along the C_{2v} insertion path.

Fig. 8 shows, for C_{2v} geometries, a plot of the three-body extended Hartree–Fock energy as a function of characteristic bond distance R. For $\alpha = 60°$, we observe a change of sign from negative to positive values at about $R = 2\ a_0$ then followed by a maximum at $R \simeq 2.3\ a_0$ and a sudden decrease to values close to zero for geometries with $R \geqslant 3.5\ a_0$. For other values of the included angle, the notable feature is the fact that $V_{\text{EHF}}^{(3)}$ remains negative over the most important regions of R-space.

As already noted, other interesting attributes are the non-additivity ratios in eqn. (19). This property has a clear theoretical bearing (see refs. 12 and 13) being especially relevant for nonbonded triatomic systems such as $H_3(^4A')$, which have also unbound asymptotic channels. Figs. 9 and 10 show the calculated HF ratios, and hence complement Figs. 3 and 4 which have been introduced earlier in this work. Recall that both Figs. 3 and 4 show the HF non-additivity ratios for C_{2v} geometries keeping fixed the included angle. In particular, note from Fig. 3, that there is a sign change of η_{HF} (from negative to positive values) which occurs only for large opening angles, and hence is most clear for $D_{\infty h}$ geometries. Note further that the most negative ratios occur for D_{3h} geometries with $R \simeq 2.5\ a_0$. These results may be rationalized from the

behaviour of $V_{\text{EHF}}^{(3)}$, and the fact that the two-body HF energies are positive for most R values of interest (columns four and five of Table 3). Indeed, as shown in Fig. 4, this type of behavior has also been observed in previous calculations, with which ours are in good agreement. Specifically, Fig. 9 shows the HF non-additivity ratios for geometries of C_{2v} or higher symmetry having the same perimeter as a function of the included angle. Except for the smallest perimeter considered, $P = 6\ a_0$, there is a change of sign from negative to positive values at about $\alpha \sim 120°$. As might be anticipated, the amplitude of this sign change decreases for increasing values of R with the α-dependence becoming nearly a flat line for $P \geqslant 21\ a_0$. In turn, Fig. 10 shows a similar plot of Fig. 9 although highlighting the comparison with previous calculations. The agreement is good. In summary, our confidence in the DMBE potential energy surface for $H_3(^4A')$ stems from the fact that the functional form connects accurately and smoothly all HF energies while being formally correct at all asymptotic limits.

In relation to the FCI calculations, we show in Table 5 a comparison between the results for the two basis sets used in the present work. They are seen to be quite similar. In Figs. 11 and 12, we compare the non-additive ratios for the FCI calculations using the two basis sets. Clearly, the FCI calculations agree well with the DMBE potential energy surface. In Table 6 we report a comparison between the results of the damped triple-dipole form in eqn. (24) and the FCI ones using the
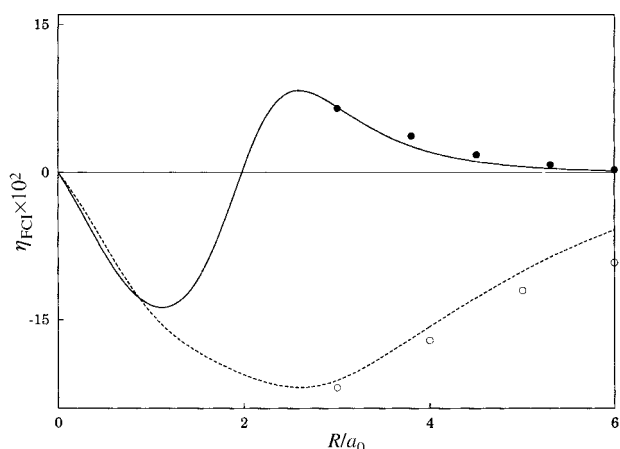
Table 6 Comparison of the triple-dipole function of eqn. (24) with the results from the FCI *ab initio* calculations using the Dunning aug-cc-pVQZ basis sets

R	Eqn. (24)	*Ab initio*[a]
D_{3h}		
3.00	$0.84127775 \times 10^{-4}$	-0.925217×10^{-4}
4.00	$0.27858134 \times 10^{-4}$	0.527659×10^{-4}
5.00	$0.78316354 \times 10^{-5}$	0.294806×10^{-4}
6.00	$0.21846667 \times 10^{-5}$	0.76519×10^{-5}
7.00	$0.65128806 \times 10^{-6}$	0.13209×10^{-5}
8.00	$0.21224411 \times 10^{-6}$	0.1201×10^{-6}
$D_{\infty h}$		
3.00	$0.13421621 \times 10^{-4}$	0.839113×10^{-4}
3.75	$-0.23271909 \times 10^{-5}$	0.184944×10^{-4}
4.50	$-0.21102076 \times 10^{-5}$	0.22315×10^{-5}
5.25	$-0.97613716 \times 10^{-6}$	-0.3805×10^{-6}
6.00	$-0.39862347 \times 10^{-6}$	-0.5265×10^{-6}

[a] This work.

Dunning basis set. Eqn. (24) is seen to agree moderately well with the results of the FCI calculations only at large distances where the triple-dipole dispersion energy is expected to dominate. A comparison of the damped triple-dipole energy from eqn. (24) with the calculated three-body dispersion energy and the triple-dipole non-additive results of Korona *et al.*[19] is presented in Fig. 13 for geometries with D_{3h} symmetry. The agreement is generally good between eqn. (24) and the results of Korona *et al.*[19] It becomes moderate between the two sets of theoretical values, especially at large separations which may be due to our basis set being much smaller than that employed in ref. 19 ([5s5p3d1f], with optimization of the exponents of the polarization functions to minimize the energy of the triplet diatomic fragment at the van der Waals minimum).

6 Conclusions

In this work we have reported a DMBE representation of the lowest-quartet potential energy surface for H_3, which has partly been based on *ab initio* restricted Hartree–Fock calculations also reported in this work. Although no direct experimental information is available to judge its reliability, the present potential energy surface should provide, together with a previously reported surface for the two sheets of ground-

Fig. 11 Comparison of non-additive ratios for the full CI calculations in the Siegbahn and Liu basis (points) set and the DMBE potential (lines): $\bigcirc$, --- 60°; $\bullet$, —— 180°.
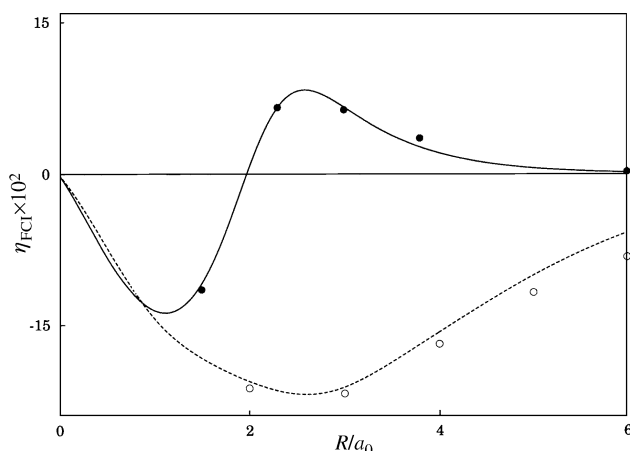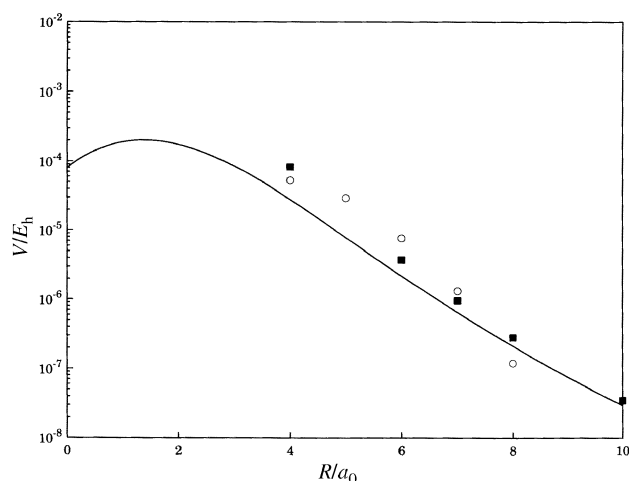

Fig. 12 Comparison of non-additive ratios for the FCI calculations in the aug-cc-pVQZ basis set of Dunning (points) and the DMBE ratios (lines): $\bigcirc$, --- 60°; $\bullet$, —— 180°.

Fig. 13 Comparison of the damped triple-dipole energy eqn. (24) (full line) with the FCI calculations using the aug-cc-pVQZ basis set of Dunning (open circles). Also shown for comparison are the results of Korona *et al.*[19] (full squares).

doublet H_3 a set of reliable and consistent potentials on which accurate dynamics calculations involving three colliding H atoms may be carried out, including theoretical studies of the thermophysical and transport properties of atomic hydrogen. Our confidence stems mainly from the semiempirical method used, which utilizes information both from standard quantum chemical calculations and from long range perturbation theory, while comprising a development of the total potential energy into two-body and three-body energy contributions and hence ensuring the correct asymptotic limit at all dissociation channels. It should be mentioned that all long-range contributions have been adequately damped to account for charge-overlap effects at regions where the breakdown of the multipolar expansion takes place. It should be noted that the comparison of the potential obtained with FCI calculations using the same basis set and a larger one show good agreement. A final comment on the smoothness of the fitted function, and quality of final DMBE potential, which have both been conveniently assessed through a number of graphical displays. In particular, plots of the ratios between three-body and two-body Hartree–Fock energy contributions as a function of various coordinates have shown that those ratios are accurately described by the functional form of the present work.

Acknowledgements

References

1 P. E. M. Siegbahn and B. Liu, *J. Chem. Phys.*, 1978, **68**, 2457.
2 A. J. C. Varandas, F. B. Brown, C. A. Mead, D. G. Truhlar and N. C. Blais, *J. Chem. Phys.*, 1987, **86**, 6258.
3 A. I. Boothroyd, W. J. Keogh, P. G. Martin and M. R. Peterson, *J. Chem. Phys.*, 1991, **95**, 4343.
4 A. J. C. Varandas and P. E. Abreu, *Chem. Phys. Lett.*, 1998, **293**, 261.
5 Y.-S. M. Wu, A. Kuppermann and J. B. Anderson, *Phys. Chem. Chem. Phys.*, 1999, **1**, 929.
6 J. N. Murrell, S. Carter, S. C. Farantos, P. Huxley and A. J. C. Varandas, *Molecular Potential Energy Functions*, Wiley, New York, 1984.
7 A. J. C. Varandas, *Adv. Chem. Phys.*, 1988, **74**, 255.
8 A. J. C. Varandas, in *Lecture Notes in Chemistry*, ed. A. Laganá, Springer-Verlag, Berlin, in press.
9 A. J. C. Varandas and J. N. Murrell, *J. Chem. Soc., Faraday Trans. 2*, 1977, **73**, 939.
10 A. J. C. Varandas, A. M. A. Rodrigues and M. A. Matías, unpublished results; A. M. M. Rodrigues, MSc Thesis, Universidade de Coimbra, Portugal, 1993.
11 T. H. Dunning, Jr., *J. Chem. Phys.*, 1989, **90**, 1007.
12 J. N. Murrell, A. J. C. Varandas and M. F. Guest, *Mol. Phys.*, 1976, **31**, 1129.
13 W. Kolos and A. Lés, *Chem. Phys. Lett.*, 1972, **14**, 167.
14 A. J. C. Varandas, in *Trends in Atomic and Molecular Physics*, ed. M. Yánez, Universidad Autonoma de Madrid, Madrid, 1990, p. 113.
15 A. J. C. Varandas, in *Dynamical Processes in Atomic and Molecular Physics*, ed. G. Delgado-Barrio, Adam Hilger, Bristol, 1992.
16 A. J. C. Varandas, *Chem. Phys. Lett.*, 1992, **194**, 333.
17 A. J. C. Varandas and J. N. Murrell, *Chem., Phys. Lett.*, 1981, **84**, 440.
18 A. J. C. Varandas and J. N. Murrell, *Faraday Discuss. Chem. Soc.*, 1977, **62**, 92.
19 T. Korona, R. Moszybski and B. Jeziorski, *J. Chem. Phys.*, 1996, **105**, 8178.
20 M. W. Schmidt, K. K. Baldridge, J. A. Boatz, S. T. Elbert, M. S. Gordon, J. H. Jensen, S. Koseki, N. Matsunaga, K. A. Nguyen, S. Su, T. L. Windus, M. Dupuis and J. A. Montgomery, *J. Comput. Chem.*, 1993, **14**, 1347.
21 V. Lewchenki, G. C. Hancock and P. R. Certain, *J. Chem. Phys.*, 1982, **76**, 3119.
22 B. H. Wells and S. Wilson, *Mol. Phys.*, 1985, **55**, 199.
23 A. J. C. Varandas and J. D. da Silva, *J. Chem. Soc., Faraday Trans.*, 1992, **88**, 941.
24 A. J. C. Varandas and A. I. Voronin, *Chem. Phys.*, 1995, **194**, 91.
25 C. Herring and M. Flicker, *Phys. Rev. A*, 1964, **134**, 362.
26 B. M. Smirnov and M. I. Chibisov, *Sov. Phys. JETP*, 1965, **21**, 624.
27 A. I. Reznikiv and S. Y. Umanskii, *Theor. Exp. Chem.*, 1971, **7**, 478.
28 A. J. C. Varandas, *J. Chem. Phys.*, 1997, **107**, 867.
29 A. J. C. Varandas, *Mol. Phys.*, 1987, **60**, 527.
30 R. J. L. Roy, *Spec. Period. Rep.: Chem. Soc. Mol. Spectrosc.*, 1973, **1**, 113.
31 W. Kolos and L. Wolniewicz, *Chem. Phys. Lett.*, 1974, **24**, 457.
32 B. S. Garbow, K. R. Hillstrom and J. J. Moore, *Documentation for the MINPACK subroutine LMDER*, Argonne National Laboratory, IL, 1980.
33 J. J. Moré, Numerical Analysis, in *Lecture Notes in Mathematics*, ed. G. A. Watson, Springer-Verlag, Berlin, 1977, vol. 630, p. 103.
34 B. M. Axilrod and E. Teller, *J. Chem. Phys.*, 1943, **11**, 299.
35 B. M. Axilrod, *J. Chem. Phys.*, 1951, **19**, 719.
36 Y. Mutto, *Proc. Phys. Soc. Jpn.*, 1943, **17**, 629.
37 S. F. O'Shea and W. J. Meath, *Mol. Phys.*, 1974, **28**, 1431.
38 A. J. C. Varandas, *Mol. Phys.*, 1983, **49**, 817.
39 W. J. Meath and R. A. Aziz, *Mol. Phys.*, 1984, **52**, 225.
40 M. Bulski, *Chem. Phys. Lett.*, 1981, **78**, 361.
41 Y. M. Chan and A. Dalgarno, *Mol. Phys.*, 1965, **9**, 525.